The Effect of Cross-section and Elliptical Hole Ratio on Crashworthiness Parameters of Crash-Box Structure

Budi Aji Warsiyanto[1], Muhammad Hadi Widanto [2], Ilham Musthofa [3], Ichsan Maulana [4], Sahril Afandi Sitompul [5], Endah Yuniarti [6]

[1,2,3,4,5,6]Prodi Teknik Penerbangan, Fakultas Teknologi Kedirgantaraan
Universitas Dirgantara Marsekal Suryadarma
Komplek Bandara Halim Perdanakusuma, Jakarta 13610, Indonesia

e-mail: budiajiwarsiyanto@gmail.com

Received: 19-09-2020. Accepted: 24-02-2021. Published: 30-06-2021

Abstract

This paper assesses computationally the thin-walled column structure with multi-cell and aluminum alloy 6061-O against dynamic compression in the axial direction. The dynamic explicit was employed in the Abaqus code to study characteristics of the cross-section differences. The complex proportional assessment (COPRAS) method was employed to determine a configuration that complies with the indicator parameters. The chosen cross-section configuration is further enhanced by creating elliptical holes with different diameter ratios. The results show that the thin-walled column structure with a nine-cell cross-section accompanied by an elliptical hole ratio of 0.3 indicates the potential corresponding to the indicator parameters for the crashworthiness application.

Keywords: *thin-walled column, cross-section, crashworthiness, hole, complex proportional assessment*

1. Introduction

Crashworthiness is the ability of the vehicle structure to experience deformation due to controlled crashing forces to protect passengers. Crashworthiness is also highly dependent on how the materials, construction, and design of the vehicle (Daehn, 2014).

The thin-walled column structure is used as energy absorbers and widely applied in the field of transportation, aerospace, military equipment, and other industries which have the advantages of lightweight, energy absorption capacity, low price, high strength, and stiffness (Sun et al., 2015). The thin-walled column structure is usually found in the part that functions to withstand the impact load as shown in Figure 1-1. Thin-walled columns with AA6061-O material were found to be an efficient energy-absorbing component (Zhang & Zhang, 2013).

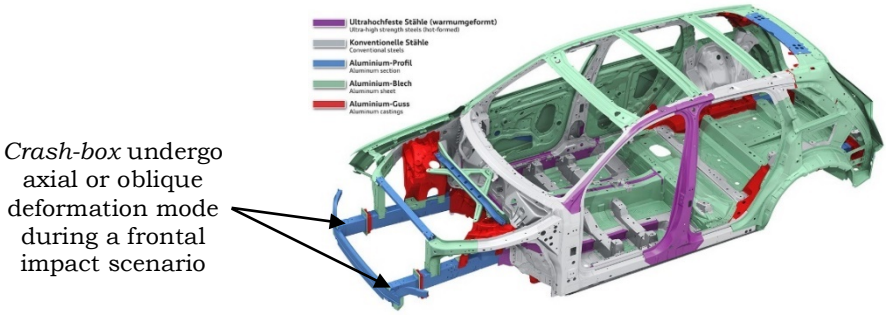

Figure 1-1: Crash-box location on vehicle structure (Baroutaji et al., 2017)

Previously, the energy-absorbing behavior of thin-walled structures has been conducted under axial and oblique loading in many studies (Baroutaji et al., 2017). A difference of the thin-walled column structures with different cross-sections such as circular, rectangle, square, hexagonal, octagonal, and ellipse (Tarlochan et al., 2013).

In 2014 – 2018, 144000 deaths were reported due to accidents in Indonesia (BPS-Statistics, 2018). The traffic accident death rate per 100,000 population stands at 12. This figure shows a very high rate compared to Singapore with 4.8 and Australia 5.2. Most researchers assume that the traffic accident death rate in Indonesia is still not fully reported. Also, the data are inconsistent and difficult to verify. Based on the trend of traffic accident death data, it is estimated that in 2020 traffic accident deaths in Indonesia will reach 40,000 per year. In fact, for the year 2035, it is estimated that there will be 65,000 traffic accident deaths per year.

Crash-box research has been carried out extensively with various cross-section configurations to obtain high energy absorption ($\boldsymbol{EA}$) and low peak crushing force ($\boldsymbol{F_{max}}$), both by numerical and experimental methods. Several researchers, such as (Chen & Wierzbicki, 2001) conducted tests on one-, two-, and three-cell columns. The test results show that the energy absorption efficiency of the three-cell column (Figure 1-2 (a)) is higher than that of the one- and two-cell columns. (Kim, 2002) optimized multi-cell cross-section configuration with four elements in each corner. The results show that the cross-section configuration of the four square elements (Figure 1-2 (b)) has a higher EA value than the circular elements. (Hou et al., 2008) conducted research on the column structure with one-, two-, three-, and four-cell cross-sections. The results show that the four-cell cross-section increases EA and minimizes F_{max} as shown in Figure 1-2 (c). (Zhang & Cheng, 2007) conducted a numerical study of the energy absorption characteristics between foam-filled square columns and multi-cell square columns. The results showed that the nine-cell column as shown in Figure 1-2 (d) was 50-100% more efficient in absorbing energy than the column filled with foam. (Najafi & Rais-Rohani, 2011) conducted tests on multi-cell cross-sections with web and corner optimization. The results show that the web-to-web cross-section (Figure 1-2 (e)) has the highest EA and lowest F_{max}. Additionally, (Rabeta & Sitompul, 2018) adds a circle and ellipse hole to the single wall crash-box to reduce F_{max}. It was found that the elliptical hole has a smaller F_{max} value than the circular hole. However, no studies have been published on the comparison of the best multi-cell of the thin-walled column structure as shown in Figures 1-2 with added holes.

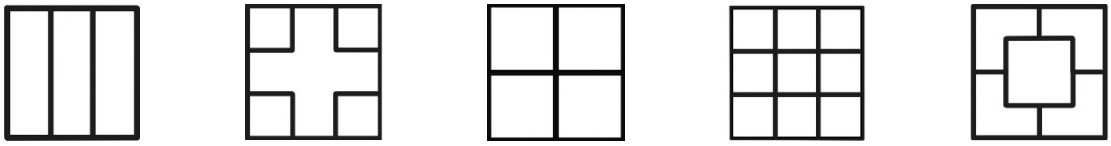

(a) (b) (c) (d) (e)

Figure 1-2: Cross-section configurations of thin-walled column structures, (a) (Chen & Wierzbicki, 2001), (b) (Kim, 2002), (c) (Hou et al., 2008), (d) (Zhang & Cheng, 2007), (e) (Najafi & Rais-Rohani, 2011)

Based on several previous studies, this study performed using the numerical method. For impact research, numerical methods can provide convenience in understanding the deformation mechanism and the response of the energy-absorbing column against an impact load. Numerical methods can reduce the need for prototype manufacturing which tends to be expensive for physical testing and helps in cases of comparisons and differences in designs. Therefore, the novelty of this research was to determine the best multi-cell of the thin-walled structures and ratio of elliptical holes based on crashworthiness indicator parameters.

2. Performance Parameter

Parameters that become indicators to determine the best cross-section based on (Baroutaji et al., 2017) as follows:

- *Peak crushing force,* $\boldsymbol{F_{max}}$

Peak crushing force is the highest force/load required to cause significant deformation. The peak crushing force is measured from the reaction force on the fixed base, which is the same principle as to how load cells are used in physical testing.

- *Energy absorption,* $\boldsymbol{EA}$
  Energy absorption is the energy absorbed by the structure to deform during an impact. The total energy absorbed by the structure is equal to the area under the instantaneous force-displacement curve as formulated as follows:

$$EA = \int_0^{dmax} FdS \tag{2-1}$$

  d_{max} and F is the maximum deformation and instantaneous force. The higher the EA value, the higher the structure's ability to absorb impact energy.

- *Mean crushing force,* $\boldsymbol{F_{mean}}$
  Mean crushing force is the mean force experienced by the structure when it is deformed. Mathematically, F_{mean} can be formulated as follows:

$$F_{mean} = \frac{EA}{d} \tag{2-2}$$

  F_{mean} optimal occurs when the value tends to be equal to the value of F_{max}.

- *Crushing force efficiency,* $\boldsymbol{CFE}$
  Crushing force efficiency is the ratio of F_{mean} and F_{max}. F_{mean} and F_{max} are important parameters to be determined because they are directly related to the decelerations that will be experienced by vehicle passengers. If the ratio approaches unity (value 1), then the F_{mean} a value close to the F_{max} the value thus minimizing the change in decelerations. In other words, if this ratio is far from unity, there is a rapid change in deceleration and this is dangerous when applied to crashworthiness design. In general, the CFE value is closer to one, the better its ability to absorb energy. Mathematically, CFE can be formulated as follows:

$$CFE = \frac{F_{mean}}{F_{max}} \tag{2-3}$$

To determine the best cross-section configuration, a multi-criteria decision making (MCDM) process is used with a complex proportional assessment (COPRAS) method as chosen by (Dehghan-Manshadi et al., 2007), (Chatterjee et al., 2011), and (Huang & Xu, 2019) in their research. This method was chosen because it is relatively easy to use. This method is related to differences in the criteria for the indicator parameters and the weight of each criterion for the indicator parameters. The COPRAS method has successfully solved design selection problems in many fields, such as construction, project management, and economics. This method consists of many steps which are described as follows:

Step 1: Creating the initial matrix (X). This first step involves creating a simple matrix that maps out design concepts for the selection of parameter criteria. This matrix is denoted as X whose writing is given as follows:

$$X = \left[x_{ij}\right]_{mXn} = \begin{bmatrix} x_{11} & x_{12} & \cdots & x_{1n} \\ x_{21} & x_{22} & \cdots & x_{2n} \\ \vdots & \vdots & \vdots & \vdots \\ x_{m1} & x_{m2} & \cdots & x_{mn} \end{bmatrix} \tag{2-4}$$
$$(i = 1,2 \cdots m), (j = 1,2 \cdots n)$$

x_{ij} is the value of component i in j component, m the number of design concepts being compared and n is the number of parameters.

Step 2: Determine the relative coefficient of normalization matrix R. The design selection problem is that many design parameters do not have the same dimensions or units. This makes the selection a little more difficult.

One way to solve this problem is to convert the entire matrix X to a non-dimensional matrix R. This makes it is easier to compare and select design concepts based on indicator

parameters. The symbol x_{ij}represents a positive (absolute) value for each parameter and $\sum x_{ij}$ is the sum of the values for one of the design concepts. The purpose of the relative coefficient is to reduce or simplify the parameter values so that they are easier to compare. The relative coefficient symbol is R which is formulated as follows:

$$R = [r_{ij}]_{mXn} = \frac{x_{ij}}{\sum_{i=1}^{m} x_{ij}} \quad (2\text{-}5)$$

Step 3: Determine the weight of each parameter which is described as follows:

Compare the two parameters. Total comparison sets (N) are equal to $N = (n(n-1)/2)$, where n is the number of parameters. In this study, $n = 3$ which represents the parameters F_{max}, EA, and CFE.

Between the two selected parameters, give a score on each criterion of the indicator parameter. For more important parameters, a score of 3 is given, while less important parameters are given a score of 1. In this study, the score $N_{ij} = 3$ for F_{max} and EA, while $N_{ij} = 1$ for CFE.

The total number of scores obtained for each parameter (W_j) is shown in equation (2-6), then calculate the weight of each parameter (w_j) with equation (2-7).

$$W_j = \sum_{i=1}^{m} N_{ij} \quad (2\text{-}6)$$

$$w_j = \frac{W_j}{\sum_{j=1}^{n} W_j} \quad (2\text{-}7)$$

Step 4: Calculating the normalized weight of matrix D.

$$D = [d_{ij}] = r_{ij}\ x\ w_j \quad (2\text{-}8)$$

d_{ij} is the normalization of the weight value of the component design concept i with the parameter j.

Step 5: Determine and summing the weighted normalized values for the beneficial and non-beneficial parameters, which are shown as follows:

$$S_{+i} = \sum_{i=1}^{n} d_{+ij} \quad (2\text{-}9)$$

$$S_{-i} = \sum_{i=1}^{n} d_{-ij} \quad (2\text{-}10)$$

d_{+ij} an d_{-ij} are the weighted normalized values for beneficial and non-beneficial elements.

Step 6: Determine relative significance or priority. The design concept priority is calculated based on the relative significance (Q_i). The larger the Q_i value, the greater the priority of the design concept. The design concept with the maximum relative significance value (Q_{max}) is the best choice for concept selection decisions. Relative significance is formulated as follows:

$$Q_i = S_{+i} + \frac{S_{-min} \sum_{i=1}^{m} S_{-i}}{S_{-1} \sum_{i=1}^{m} (S_{-min}/S_{-i})} \quad (2\text{-}11)$$

Step 7: Calculate the quantitative utility (U_i) for the design concept. Quantitative utility values are directly related to relative significance. The quantitative utility value determines the rating of the design concept which can be calculated by dividing the priority of each design concept by the maximum value. Mathematically, the quantitative utility can be written as follows:

$$U_i = \frac{Q_i}{Q_{max}} \quad (2\text{-}12)$$

The maximum value of relative significance is denoted as Q_{max}.. The quantitative utility value (U_i) 100 is considered to be the best design concept.

3. Methodology

This research is divided into two phases. In the first phase, five columns with different cross-sections were designed. The cross-section differences consisted of three-cell [3S], four square elements [4P], nine-cell [9S], four-cell [4S], and web-to-web [WW] with AA6061-O material (Kumar et al., 2018).

Column length (L) and thickness (t) was kept constant for the five cross-section configurations, namely 180 mm (Jusuf et al., 2015) and 1 mm, respectively. Next, the best cross-section will be selected based on parameter values using the COPRAS method.

The second phase is to further improve the crash performance of the selected cross-sections. Crash performance is improved by adding elliptical holes having different diameter ratios. These results will be compared and selected after going through an assessment process (COPRAS method). The initial impact speed was 3.74 ms^{-1} with an impactor mass of 290 kg (Jusuf et al., 2015). The configuration and dimensions of the column are shown in Figure 3-1 and Table 3-1.

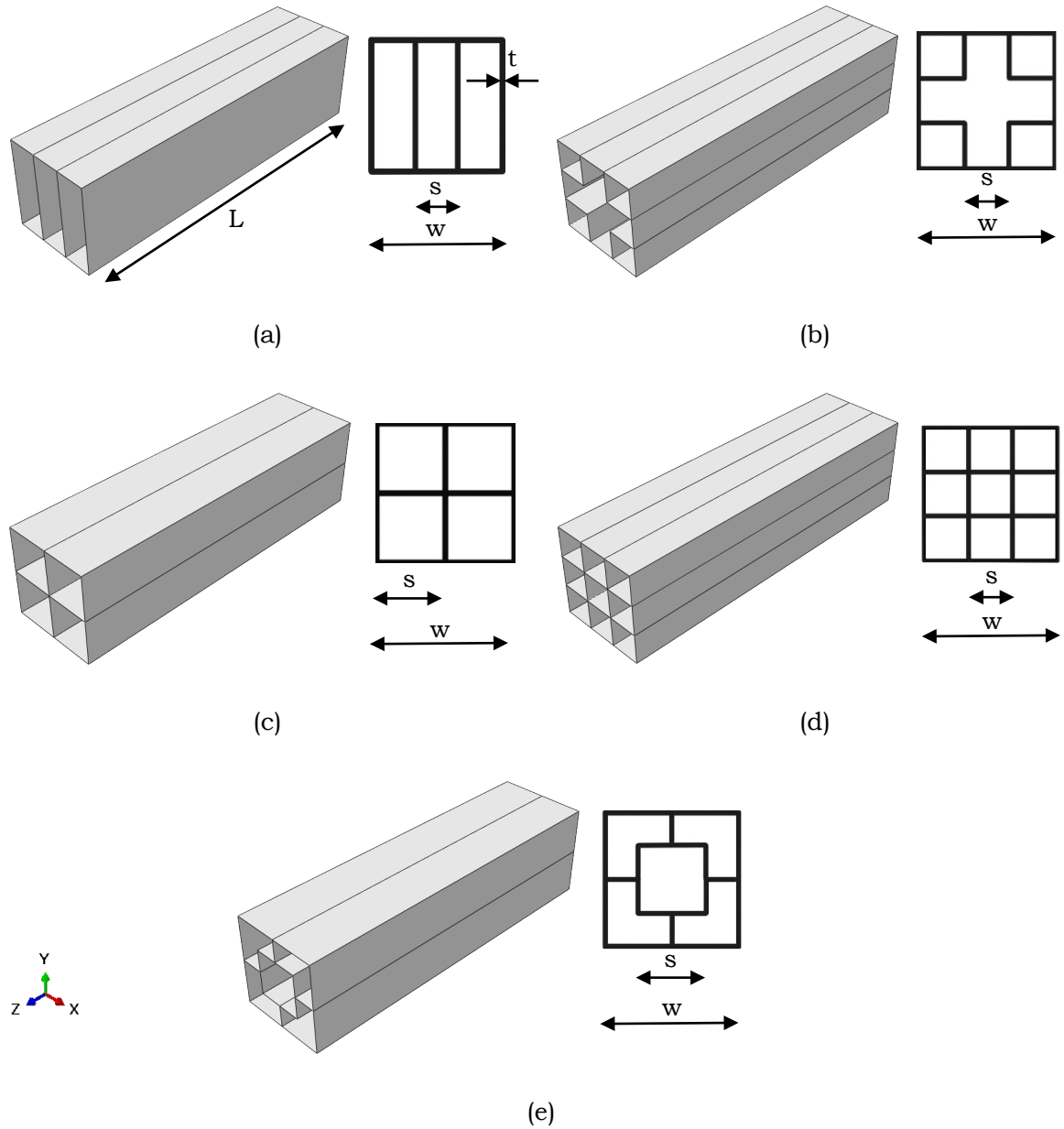

Figure 3-1: Cross-Section Configuration of Thin-Walled Column Structures: (a) Three-Cell, (b) Four Square Elements, (c) Four-Cell, (d) Six-Cell, and (e) Web-to-Web

Table 3-1: Thin-Walled Column Dimensions for Cross-Section Difference

Code		Outer wall width (mm), *w*	Inner wall width (mm), *s*
3S		48	@16
4P			
9S			
4S			@24
WW			

4. Finite Element Modeling

In this study, the finite element model is simulated using Abaqus-explicit. The entire model consists of a thin-walled column structure, impactors, and base as shown in Figure 4-1. The column structure is modeled using a 4 node shell continuum (S4R) element with 5 integration points along the direction of the element thickness. Enhanced hourglass control is used to prevent artificial zero energy deformation mode and integration point is used to prevent volumetric locking.

An element size of 2x2 mm^2 (8640 elements) was selected for the column based on the convergence mesh. The converged mesh was carried out to ensure that the mesh size was sufficient to accurately illustrate the deformation process. The convergence mesh result of the column model is shown in Figure 4-2. The contact algorithm is a "general contact" that is used to avoid column wall interpenetration. However, the computation time to be longer than other algorithms. The friction coefficient is determined to be 0.57 (Jusuf et al., 2015).

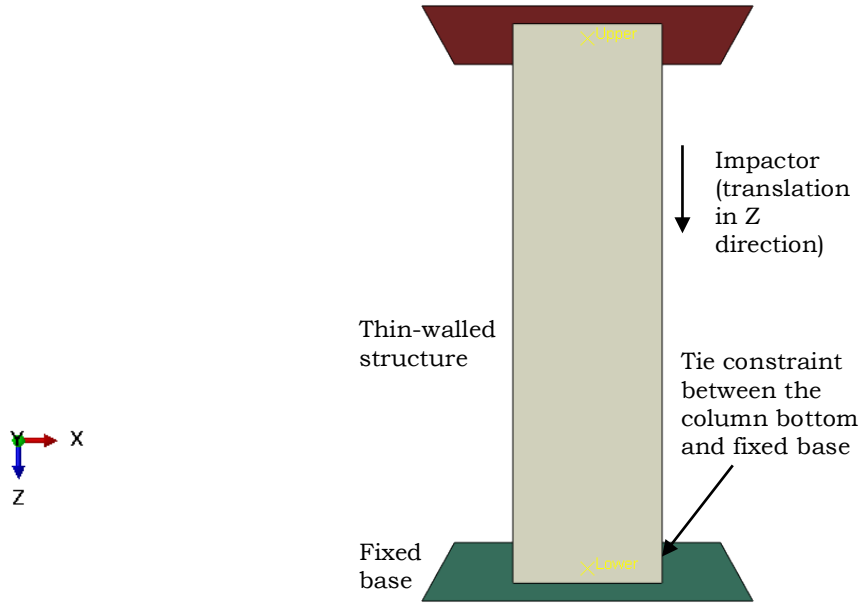

Figure 4-1: Finite Element Analysis Setup

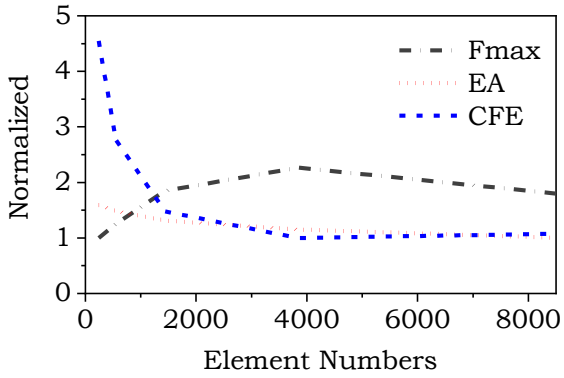

Figure 4-2: Convergence Mesh Study for Thin-Walled Model

The rigid body was employed to model the impactor. Translational displacement of the impactor only one allowable direction or in other words all other translations and rotations degree of freedom were fixed. The impact velocity of 3.74 ms-1 was chosen based on the velocity of the crash test equipment owned by the Bandung Institute of Technology. The mass of the impactor is assumed to be 25% of the mass of the passenger car, which is 1,160 kg, which means that each energy-absorbing column structure is capable of absorbing kinetic energy equivalent to the mass of 290 kg because the maximum energy that can be absorbed by the two-column structures in its application is less than 50% (Witteman, 1999). Aluminum alloy (AA6061-O) was chosen because of its ductile nature so that it is good in energy absorption applications characterized by plastic deformation. The mechanical properties of these materials are shown in Table 4-1.

Table 4-1: Mechanical Properties of AA6061-O (Zhang & Zhang, 2013)

Density ($kg.m^{-3}$)	Elastic Modulus (GPa)	Poisson's Ratio	Yield Strength (MPa)	Ultimate Strength (MPa)	Failure Strain
2.700	68	0,33	71	130,7	0,22

5. Result and Discussion

A summary of the results obtained in this study is presented in Table 5-1. The table also displays the results calculated value using the COPRAS method. The simulation results are only located in the X matrix column, while the normalized decision matrix and weighted normalized decision matrix are results calculated using the COPRAS method. A detailed discussion will be explained in the next subsection.

Table 5-1: The Decision Matrix X, Normalized, and Weighted for Profile Differences

Code		Matrix X			Normalized Matrix			Weighted Matrix		
		F_{max} (kN)	EA (kJ)	CFE	F_{max}	EA	CFE	F_{max}	EA	CFE
3S		25,10	1,77	0,54	0.1376	0.1793	0.1571	0.0574	0.0748	1.0569
4P		40,30	2,03	0,77	0.2210	0.2057	0.2214	0.0921	0.0858	0.7499
4S		31,10	2,01	0,63	0.1705	0.2036	0.1818	0.0711	0.0849	0.9130
9S		48,92	2,03	0,78	0.2682	0.2057	0.2267	0.1118	0.0858	0.7323
WW		36,97	2,03	0,74	0.2027	0.2057	0.2131	0.0845	0.0858	0.7791

5.1 Force vs. Displacement Characteristics of Different Cross-Section

The deformation of the column structure after experiencing the impact force is shown in Figure 5-1. It can be seen that the amount of progressive buckling in each cross-section configuration is different. This is due to the different inertia in each cross-section configuration. In the 3S cross-section, almost the entire column structure experiences

deformation which indicates a potential hazard when applied to the vehicle structure because it is unable to completely absorb the impact energy. The cross-section configuration with the least deformation (progressive buckling) is the 9S cross-section.

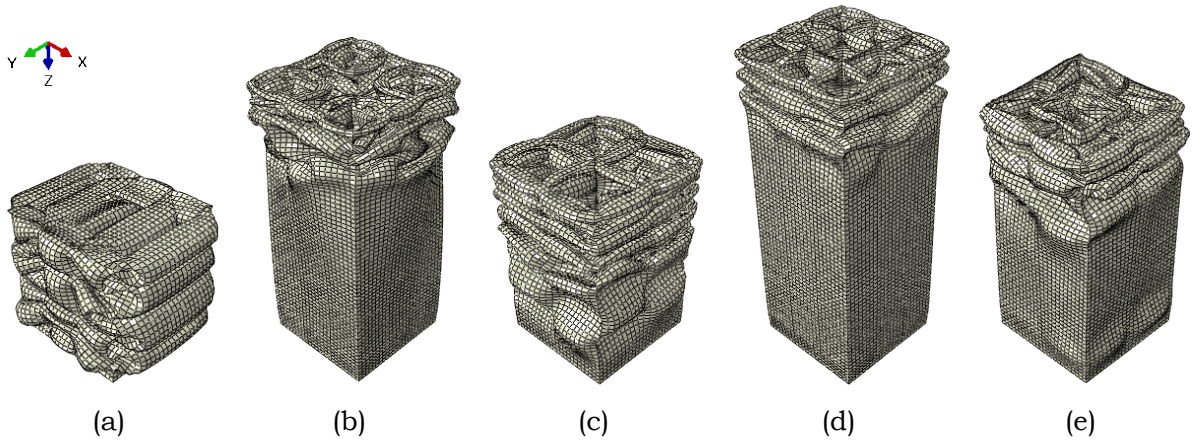

Figure 5-1: Deformation of Thin-Walled Columns After Experiencing Impact Loads for Cross-Section Differences: (a) 3S, (b) 4P, (c) 4S, (d) 9S, dan (e) WW

The instantaneous force to displacement profile for each cross-section is shown in Figure 5-2 (a). The value of the force is obtained from the reference point found on the base component with the description "Lower", while the displacement is obtained from the reference point in the impactor component with the description "Upper" as shown in Figure 4-1. The force on the base component is the reaction force due to the impact of the impactor component with a thin-walled column structure, while the displacement is obtained based on the movement of the impacting component which is in contact with the column structure. Figure 5-2 (b) shows the mean crushing force profile experienced by the column structure. From the two figures, it can be seen that the highest and lowest energy absorption (area under the curve) is found in the 9S and 3S cross-section configurations.

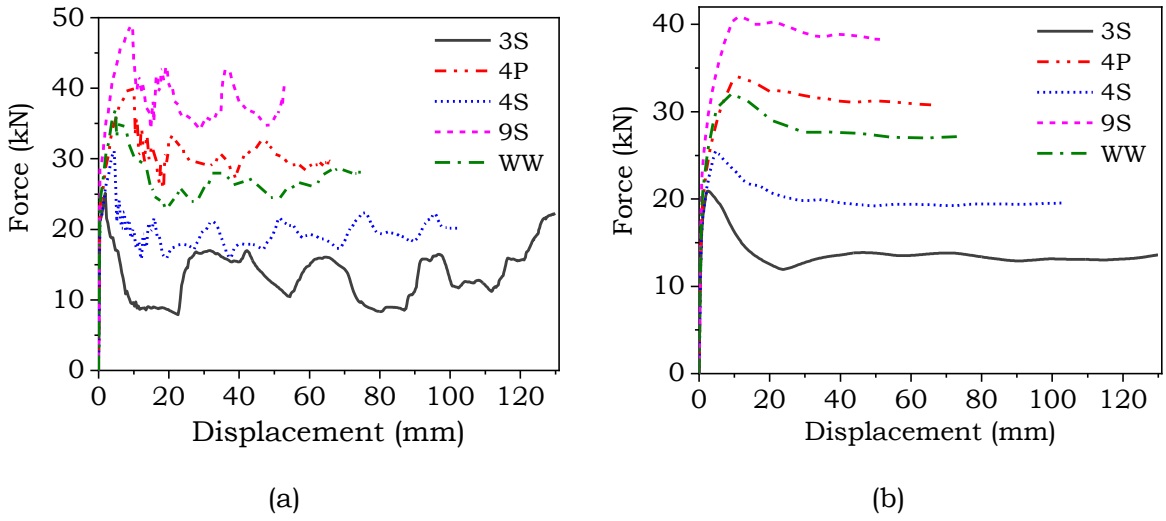

Figure 5-2: (a) Instantaneous Force vs. Displacement and (b) Mean Crushing Force vs. Displacement for Difference of the Cross-Section

5.2 Energy Absorption

In Figure 5-3, the energy absorption is plotted as a function of displacement length rather than as a function of time because to determine the energy absorption at each displacement. It is concluded that the four cross-sections (4P, 4S, 9S, and WW) have

relatively the same energy absorption value, namely, 2.02 kJ, while the three-cell (3S) cross-section has the lowest value, namely 1.80 kJ.

The next process is to choose the best column based on the crashworthiness parameters. This process involves three indicator parameters, namely peak crushing force (F_{max}), energy absorption (EA), and crushing force efficiency (CFE) which will be discussed in the next section.

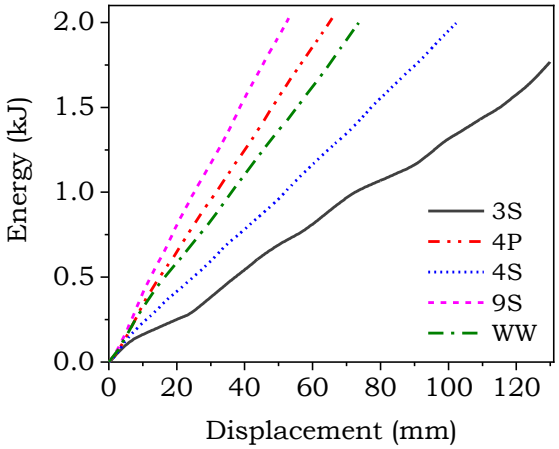

Figure 5-3: Energy Absorption Characteristics of Five Different Cross-Section

5.3 Selection of the Best Cross-Section

To determine the best cross-section, the COPRAS method is used. This method was chosen for the simplification of usability. The indicator parameters used in the cross-section selection are F_{max}, EA, and CFE.

Step 1: determine the X matrix, Step 2: determine the relative coefficient (R)normalized matrix, and Step 3: determine the weight of each indicator parameter. To get the values in step 3, need to adjust the weights from Table 5-1. It can be seen that the highest weight setting is 3 and the lowest is 1. The results of the three initial steps are shown in Table 5-2. Next, step 4 can be carried out: calculating the weighted normalized matrix (D). Step 5: determining the weighted normalized value for beneficial and non-beneficial elements. The beneficial element consists of the parameters F_{max} and EA, while the non-beneficial element is the only CFE. Step 6: determining the relative significance or priority and step 7: calculating the quantitative utility. The values of the four final steps are shown in Table 5-3.

Table 5-2: Weightage Setting for Each Crashworthiness Criteria (Huang & Xu, 2019)

Selection Criteria	**Number of Comparison Sets, $N = (3(3-1)/2 = 3)$**			W_j	w_j
	1	**2**	**3**		
F_{max}	2	3		5	5/12 = 0,417
EA	2		3	5	5/12 = 0,417
CFE		1	1	2	2/12 = 0,166
	Total, Σ			12	1

Table 5-3: Results of the COPRAS Method for Profile Differences

Code		***Beneficial S_{+i}***	***Non-beneficial S_{-i}***	Q_i	U_i	***Rank***
3S		0.1322	1.0569	0.7967	68.8796	5
4P		0.1779	0.7499	1.1146	96.3569	2
4S		0.1560	0.9130	0.9253	79.9927	4
9S		0.1976	0.7323	1.1567	100.0000	1
WW		0.1703	0.7791	1.0718	92.6586	3

Based on Table 5-3, it is found that the column structure with the 9S cross-section has the best results, followed by 4P and WW and the smallest value is 3S. Thus, a column with a cross-section of 9S was selected to investigate the defect effect in the form of an elliptical hole based on the criteria for the crashworthiness parameter.

5.4 Effect of Elliptical Holes

An elliptical hole was used to reduce F_{max} and to encourage progressive buckling in the area around the hole. An elliptical hole is created in the center of the 9S column by a total of four from the side to the side as shown in Figure 5-4 (a).

The elliptical holes are created with the difference in the ratio a/w (0.1; 0.2; 0.3; 0.4) and a constant a/b ratio (2) which details are shown in Table 5-4. As mentioned in the Introduction, elliptical holes are selected based on research (Rabeta & Sitompul, 2018) which states that the elliptical is more effective in reducing F_{max} than the circle shape.

The simulation results of the difference in the ratio of the elliptic hole diameter (a/w) for the instantaneous force to displacement parameter are shown in Figures 5-5 (a), (b), and (c). In each figure, the instantaneous and mean force profiles are displayed as well as an illustration of the thin-walled column structure when it is subjected to impact loads which cause plastic deformation (energy absorption). The stress concentration occurs in the area around the hole marked in red at the initial of the impact causing progressive buckling. Based on Table 5-5, F_{max} decreased from 48.92 kN (without holes) to 40.39 kN (hole ratio 0.3). Energy absorption tends to be constant, at 2.03 kJ. CFE increased from 0.78 for columns without holes to 0.88 for columns with a hole ratio of 0.3.

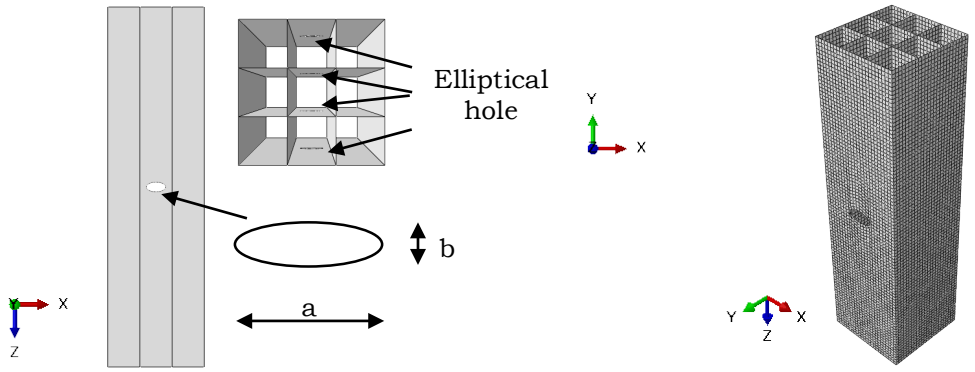

Figure 5-4: Thin-Walled Column Structure with 9S Cross-Section and Elliptical Holes: (a) Geometry dan (b) *Mesh*

Table 5-4: Elliptical Hole Dimensions

a/w	a (mm)	w (mm)	b (mm)
0,1	4,8		2,4
0,2	9,6	48	4,8
0,3	14,4		7,2

As with the previous section (cross-section differences), the COPRAS method was used to determine the best elliptic hole ratio (steps are shown in Tables 5-5 and 5-6). It is found that the column with a hole ratio of 0.3 ranks one of the three models being compared. Ranks two and three are the models with a hole ratio a/w of 0.2 and 0.1, respectively.

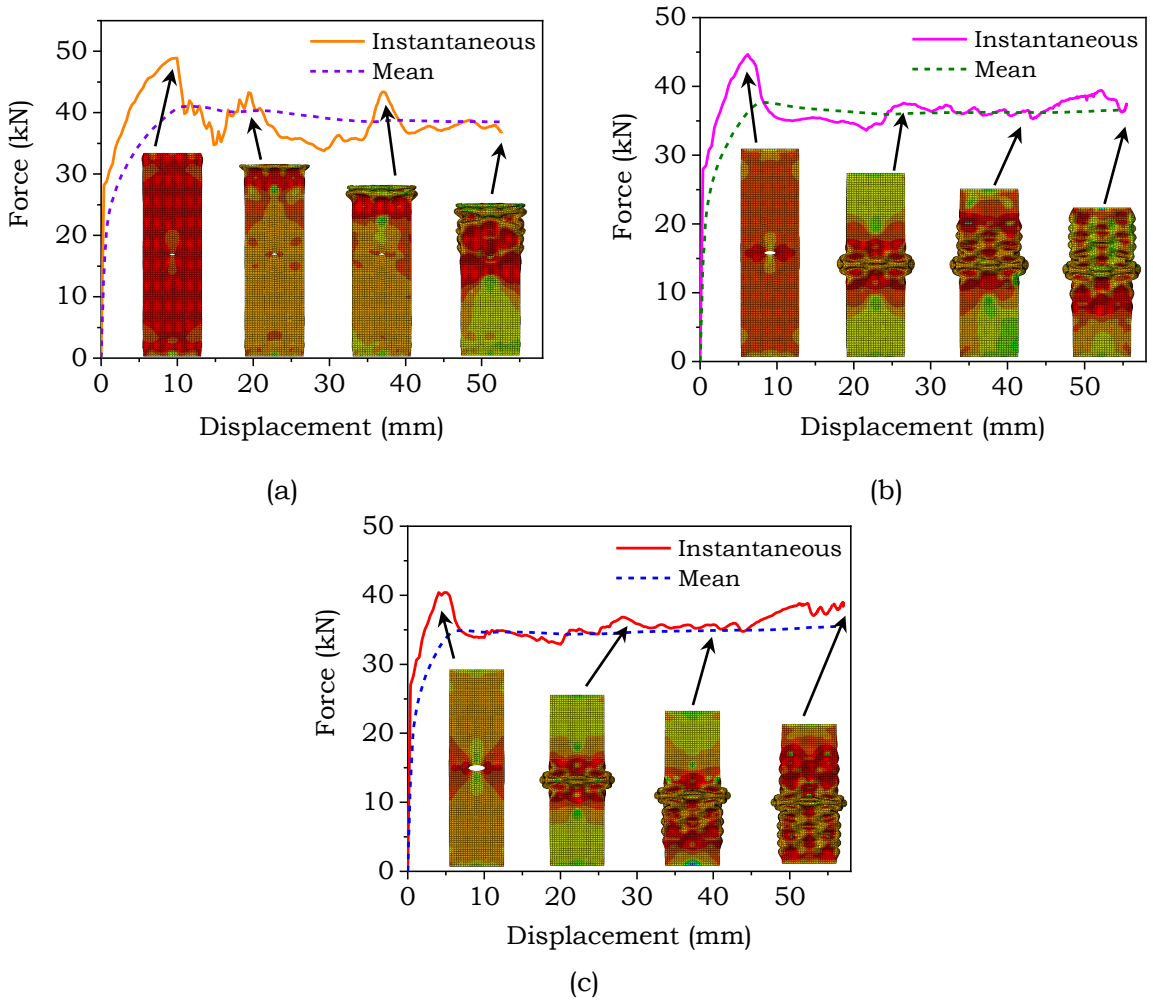

Figure 5-5: Force vs. Displacement Profile in a 9S Cross-Section with a Hole Ratio: (a) 0.1, (b) 0.2, and (c) 0.3

Table 5-5: The Decision Matrix X, Normalized, and Weighted for Hole Ratio Differences

Hole Ratio	Matrix X			Normalized Matrix			Weighted Normalized		
	F_{max} (kN)	EA (kJ)	CFE	F_{max}	EA	CFE	F_{max}	EA	CFE
0,1	48,93	2,03	0,79	0,3652	0,3341	0,3173	0,1523	0,1393	0,5231
0,2	44,65	2,03	0,82	0,3333	0,3334	0,3294	0,1390	0,1390	0,5039
0,3	40,39	2,02	0,88	0,3015	0,3325	0,3532	0,1257	0,1387	0,4699

Table 5-6: Results of the COPRAS Method for Hole Ratio Differences

Hole Ratio	*Beneficial* S_{+i}	*Non-beneficial* S_{-i}	Q_i	U_i	*Rank*
0,1	0,2916	0,5231	0,7667	96,6658	3
0,2	0,2780	0,5039	0,7711	97,2221	2
0,3	0,2644	0,4699	0,7931	100,0000	1

6. Conclusion

Numerical investigations of the axial impact response of thin-walled column structures and ductile metal alloy (AA6061-O) materials with different cross-sections and elliptical hole diameter ratios were carried out. It was found that the nine-cell cross-section (9S) was best for crashworthiness applications based on the parameters F_{max}, EA, and CFE. Also, the addition of an elliptical hole reduces the F_{max} value and increases the

CFE. This is due to the progressive buckling process which is more effective in the area around the hole. Therefore, it is concluded that the nine-cell (9S) cross-section with an elliptical hole ratio of 0.3 shows good potential for crashworthiness applications so that can reduce serious injuries to passengers in the vehicle.

Acknowledgment

This research was supported by Mr. Prio Adhi Setiawan as a Senior Advisor at the German Indonesian Association of Experts and Scholars.

References

Baroutaji, A., Sajjia, M., & Olabi, A. G. (2017). On the Crashworthiness Performance of Thin-Walled Energy absorbers: Recent Advances and Future Developments. *Thin-Walled Structures*, *118*(May), 137–163. https://doi.org/10.1016/j.tws.2017.05.018

BPS-Statistics. (2018). *Land Transportation Statistics 2018. BPS RI*.

Chatterjee, P., Athawale, V. M., & Chakraborty, S. (2011). Materials selection using complex proportional assessment and evaluation of mixed data methods. *Materials and Design*. https://doi.org/10.1016/j.matdes.2010.07.010

Chen, W., & Wierzbicki, T. (2001). Relative merits of single-cell, multi-cell, and foam-filled thin-walled structures in energy absorption. *Thin-Walled Structures*, *39*, 287–306. https://doi.org/10.1016/S0263-8231(01)00006-4

Daehn, G. S. (2014). Sustainable design and manufacture of lightweight vehicle structures. In *Alternative Fuels and Advanced Vehicle Technologies for Improved Environmental Performance: Towards Zero Carbon Transportation*. https://doi.org/10.1533/9780857097422.2.433

Dehghan-Manshadi, B., Mahmudi, H., Abedian, A., & Mahmudi, R. (2007). A novel method for materials selection in mechanical design: Combination of non-linear normalization and a modified digital logic method. *Materials and Design*. https://doi.org/10.1016/j.matdes.2005.06.023

Hou, S., Li, Q., Long, S., Yang, X., & Li, W. (2008). Multiobjective Optimization of Multi-Cell Sections for the Crashworthiness Design. *International Journal of Impact Engineering*, *35*(11), 1355–1367. https://doi.org/10.1016/j.ijimpeng.2007.09.003

Huang, H., & Xu, S. (2019). Crashworthiness Analysis and Bionic Design of Multi-Cell Tubes Under Axial and Oblique Impact Loads. *Thin-Walled Structures*, *144*. https://doi.org/10.1016/j.tws.2019.106333

Jusuf, A., Dirgantara, T., Gunawan, L., & Putra, I. S. (2015). Crashworthiness analysis of multi-cell prismatic structures. *International Journal of Impact Engineering*. https://doi.org/10.1016/j.ijimpeng.2014.11.011

Kim, H. S. (2002). New Extruded Multi-Cell Aluminum Profile for Maximum Crash Energy Absorption and Weight Efficiency. *Thin-Walled Structures*, *40*(4), 311–327. https://doi.org/10.1016/S0263-8231(01)00069-6

Kumar, A. P., Mohamed, M. N., Jusuf, A., Dirgantara, T., & Gunawan, L. (2018). Axial Crash Performance of Press-Formed Open and End-Capped Cylindrical Tubes – A Comparative Analysis. *Thin-Walled Structures*, *124*, 468–488. https://doi.org/10.1016/j.tws.2017.12.037

Najafi, A., & Rais-Rohani, M. (2011). Mechanics of Axial Plastic Collapse in Multi-Cell, Multi-Corner Crush Tubes. *Thin-Walled Structures*, *49*(1), 1–12. https://doi.org/10.1016/j.tws.2010.07.002

Rabeta, B., & Sitompul, S. A. (2018). Analysis Numerical Discontinuity of Thin-Walled Tube Subjected Low-Velocity Impact. *SENATIK 2018*, *4*(Prosiding Seminar Nasional Teknologi Informasi dan Kedirgantaraan). https://doi.org/10.28989/senatik.v4i0.144

Sun, G., Tian, X., Fang, J., Xu, F., Li, G., & Huang, X. (2015). Dynamical bending analysis and optimization design for functionally graded thickness (FGT) tube. *International Journal of Impact Engineering*, *78*, 128–137. https://doi.org/10.1016/j.ijimpeng.2014.12.007

Tarlochan, F., Samer, F., Hamouda, A. M. S., Ramesh, S., & Khalid, K. (2013). Design of thin-wall structures for energy absorption applications: Enhancement of

crashworthiness due to axial and oblique impact forces. *Thin-Walled Structures*, *71*, 7–17. https://doi.org/10.1016/j.tws.2013.04.003

Witteman, W. J. (1999). *Improved Vehicle Crashworthiness Design by Control of the Energy Absorption for Different Collision Situations* (Issue 1999). https://doi.org/10.6100/IR518429

Zhang, X., & Cheng, G. (2007). A Comparative Study of Energy Absorption Characteristics of Foam-Filled and Multi-Cell Square Columns. *International Journal of Impact Engineering*, *34*(11), 1739–1752. https://doi.org/10.1016/j.ijimpeng.2006.10.007

Zhang, X., & Zhang, H. (2013). Energy Absorption of Multi-Cell Stub Columns Under Axial Compression. *Thin-Walled Structures*, *68*, 156–163. https://doi.org/10.1016/j.tws.2013.03.014